

RESEARCH ARTICLE

10.1002/2017JB014099

Key Points:

- The 3-D CFD-DEM study of slip instabilities in saturated granular fault gouge
- Hydromechanical effect of fluid flow on characteristics of slip events
- Increased mean stress drop of slip events due to fluid hydromechanical effects

Supporting Information:

- Supporting Information S1

Correspondence to:

O. Dorostkar,
domid@ethz.ch

Citation:




Dorostkar, O., R. A. Guyer, P. A. Johnson, C. Marone, and J. Carmeliet (2017), On the role of fluids in stick-slip dynamics of saturated granular fault gouge using a coupled computational fluid dynamics-discrete element approach, *J. Geophys. Res. Solid Earth*, 122, doi:10.1002/2017JB014099.

Received 14 FEB 2017

Accepted 10 APR 2017

Accepted article online 17 APR 2017

On the role of fluids in stick-slip dynamics of saturated granular fault gouge using a coupled computational fluid dynamics-discrete element approach

Omid Dorostkar^{1,2,3} , Robert A. Guyer^{4,5}, Paul A. Johnson⁴ , Chris Marone⁶ , and Jan Carmeliet^{1,2}

¹Chair of Building Physics, Department of Mechanical and Process Engineering, Swiss Federal Institute of Technology Zurich (ETH Zurich), Zurich, Switzerland, ²Laboratory for Multiscale Studies in Building Physics, Swiss Federal Laboratories for Materials Science and Technology (Empa), Zurich, Switzerland, ³Department of Civil, Environmental and Geomatic Engineering, Swiss Federal Institute of Technology Zurich (ETH Zurich), Zurich, Switzerland, ⁴Solid Earth Geophysics Group, Los Alamos National Laboratory, Los Alamos, New Mexico, USA, ⁵Department of Physics, University of Nevada, Reno, Reno, Nevada, USA, ⁶Department of Geosciences, Pennsylvania State University, University Park, Pennsylvania, USA

Abstract The presence of fault gouge has considerable influence on slip properties of tectonic faults and the physics of earthquake rupture. The presence of fluids within faults also plays a significant role in faulting and earthquake processes. In this paper, we present 3-D discrete element simulations of dry and fluid-saturated granular fault gouge and analyze the effect of fluids on stick-slip behavior. Fluid flow is modeled using computational fluid dynamics based on the Navier-Stokes equations for an incompressible fluid and modified to take into account the presence of particles. Analysis of a long time train of slip events shows that the (1) drop in shear stress, (2) compaction of granular layer, and (3) the kinetic energy release during slip all increase in magnitude in the presence of an incompressible fluid, compared to dry conditions. We also observe that on average, the recurrence interval between slip events is longer for fluid-saturated granular fault gouge compared to the dry case. This observation is consistent with the occurrence of larger events in the presence of fluid. It is found that the increase in kinetic energy during slip events for saturated conditions can be attributed to the increased fluid flow during slip. Our observations emphasize the important role that fluid flow and fluid-particle interactions play in tectonic fault zones and show in particular how discrete element method (DEM) models can help understand the hydromechanical processes that dictate fault slip.

1. Introduction

Earthquakes, landslides, and avalanches are phenomena involving granular materials, where the stored elastic energy is suddenly released leading to potentially devastating consequences. Fault gouge, a system of granular particles created by fragmentation and wear, is believed to dictate key aspects of earthquake nucleation and dynamic rupture [Brace and Byerlee, 1966; Johnson *et al.*, 1973; Marone *et al.*, 1990]. The nature of stress accommodation and the dynamics of the stick-slip events have been well studied in laboratory experiments and numerical simulations primarily on dry granular fault gouge [Marone, 1998a, 1998b; Morgan, 1999; Mair *et al.*, 2002; Guo and Morgan, 2004; Anthony and Marone, 2005; Johnson and Jia, 2005; Mair and Hazzard, 2007; Johnson *et al.*, 2008; Samuelson *et al.*, 2008; Johnson *et al.*, 2012; Johnson *et al.*, 2013]. Recent 3-D discrete element method (DEM) numerical simulations of dry granular fault gouge demonstrate both spontaneous and triggered stick-slip [Ferdowsi *et al.*, 2013; Griffa *et al.*, 2013; Ferdowsi *et al.*, 2014, 2015] similar to experiments. There exist a few studies of fluid-saturated granular fault gouge as well. Fluids can play a significant role in the frictional strength of granular materials in the fault gouge [Scuderi *et al.*, 2014; Scuderi *et al.*, 2015a]. The effects of fluids on granular fault gouge can be divided into two categories, chemical and hydromechanical. The chemical effects include primarily pressure solution and fault healing. Pressure solution has been shown to have a substantial influence on the stick-slip behavior depending on the relative humidity of granular fault gouge, as well as chemical properties of the particles [Dieterich and Conrad, 1984; Frye and Marone, 2002; Scuderi *et al.*, 2014]. Hydromechanical effects include changes in the effective stress [Scuderi *et al.*, 2015a] and fluid-particle interactions.

The study of fluid-saturated faults has advanced recently primarily through laboratory measurements. Permeability change during seismic loading [Okazaki *et al.*, 2013; Scuderi *et al.*, 2015b; Kaproth *et al.*, 2016;

Leclère *et al.*, 2016], pressure solution, and frictional healing impacts on the stick-slip cycles as well as chemical strengthening phenomenon [Dieterich and Conrad, 1984; Losert *et al.*, 2000; Frye and Marone, 2002; Renard *et al.*, 2012; Scuderi *et al.*, 2014] have been experimentally studied in order to better understand fluid-particle interaction in faults. There has been a particular focus on fault lubrication [Bizzarri, 2012; Verberne *et al.*, 2014], pore fluid pressure [Samuelson *et al.*, 2009; Proctor and Hirth, 2015; Scuderi *et al.*, 2015a] and the granular rheology in viscous faults [Higashi and Sumita, 2009]. Considerable attention has been paid to fluid migration in fault zones in the past [Yamashita, 1999], and several mechanisms have been suggested in regard to retarding, i.e., increasing recurrence time of slip events.

Triggered seismicity due to fluid pressure has been reported recently for rock deformation experiments on carbonate rocks [Scuderi and Collettini, 2016]. One significant issue arising from experiments on granular fault gouge is the combined effect of chemical and mechanical processes in fluid-particle interaction [Niemeijer *et al.*, 2010]. There is no reported work that we are aware of that attempts to isolate these processes. The versatility of numerical modeling tools can address some of these issues. For example, one can prepare identical numerical samples in contrast to experiments, for different simulations. One can also run simulations with or without chemical or mechanical effects. Numerical simulations also offer the possibility to perform a parametric study identifying the most important parameters governing the stick-slip dynamics, to study time series of stick-slip events and eventually to try to identify the underlying mechanisms of slip from the grain-scale phenomena. Goren *et al.* [2011] studied the mechanical coupling of fluid-filled granular materials under shear with a 2-D DEM model. Both experimental and field-scale studies [Sutherland *et al.*, 2012] have shown the significance of 3-D aspects, such as particle rearrangements [Ferdowsi *et al.*, 2013] and 3-D fluid flow within a granular fault gouge [Achtziger-Zupančič *et al.*, 2016]. The size and timing of consecutive slip events are the two main characteristics of a stick-slip sequence. We are particularly interested in the influence of fluid on the size of slip events and their recurrence time. The main aim of this paper is to study these characteristics with the use of 3-D coupled computational fluid dynamics (CFD)-DEM simulations. We study the stick-slip behavior of a fluid-saturated granular fault gouge using computational fluid dynamics (CFD) and discrete element method (DEM) in a two-way coupling between particle solid and the fluid phase. Our numerical simulations allow us to analyze the hydromechanical effects of fluid flow in a fluid-saturated granular fault gouge. Such an approach enables us to compare long time series of dry and fluid-saturated granular fault gouge for identical samples.

In this paper, we present simulation results of dry and fluid-saturated granular fault gouge and analyze the effects of fluid on the released particle kinetic energy, the drop in shear stress or friction coefficient, layer thickness change, and recurrence time, in a drained granular fault gouge. We first present the numerical method and the characteristics of the stick-slip behavior of a dry granular fault gouge. We then compare characteristics of slip events, i.e., friction drop, kinetic energy release, thickness drop, and recurrence time for the dry and fluid-saturated granular fault gouge. Finally, we present a detailed analysis showing distributions of these characteristics and their relation, indicating that fluid can increase the size of slip events. We conclude that the hydromechanical effect of fluids in a granular fault gouge has to be considered showing the need for grain-scale studies in the future.

2. CFD-DEM Methodology

To simulate the stick-slip behavior of fluid-saturated granular fault gouge, we use the discrete element method (DEM) for the solid phase (particles) and computational fluid dynamics (CFD) for the fluid phase. The coupled CFD-DEM method allows for a two-way coupling taking into account the main fluid-particle interactions, i.e., momentum transfer and related forces between two phases [Goniva *et al.*, 2012]. In this section, we briefly describe the general method. For more information describing the governing equations as well as different approaches regarding modeling fluid-particle interaction, please see the cited references [Zhou *et al.*, 2010; Goniva *et al.*, 2012; Kloss *et al.*, 2012].

2.1. DEM

In DEM, first introduced by Cundall and Strack [1979], the equation of motion for each individual particle considering the force balance is solved in order to track the particles:

$$\sum F_{pi} = m_{pi} \left(\frac{d}{dt} u_{pi} \right), \quad (1)$$

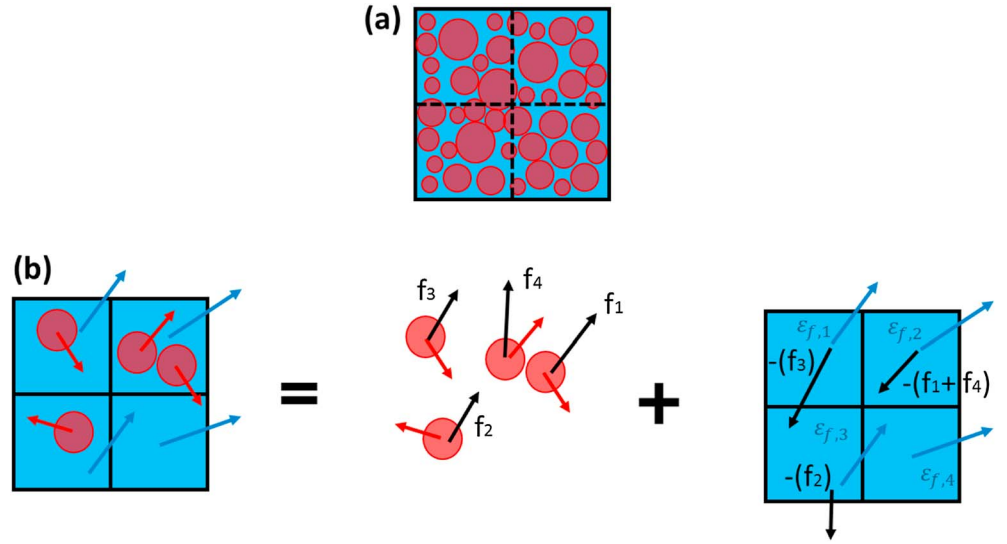


Figure 1. (a) Schematic of unresolved CFD-DEM where each CFD cell contains several solid particles (in red). (b) CFD-DEM calculations including forces on particles from the fluid plus CFD calculations considering void fraction and momentum sources. Our approach solves the coupled CFD-DEM problem simultaneously. The red arrows on particles show particle-particle interaction forces, and the blue arrows on CFD cells show their momentum vectors. The DEM solver takes into account forces from fluid on particles (black arrows, f_i force on particle i from fluid), and CFD solver includes them solving momentum equation. The porosity ($\varepsilon_{f,j}$) for each CFD cell (j) is calculated based on particles position.

$$\sum T_{pi} = I_{pi} \left(\frac{d}{dt} \omega_{pi} \right), \quad (2)$$

where m_{pi} , I_{pi} , u_{pi} and ω_{pi} stand for mass, moment of inertia, translational velocity, and angular velocity of particle i , respectively. In equations (1) and (2), F_{pi} and T_{pi} are forces and torques acting on particle i owing to particle-particle contacts as well as body forces. In a fluid-saturated system, fluid-particle interaction forces have to be added to these forces as will be explained in the following section. The contacts between particles in soft sphere DEM is attained by allowing particle overlap. The resulting contact law is based on interaction of several interconnected rheological elements, i.e., elasticity (spring) and viscosity (dashpot). The spring stores the elastic energy, while the dashpot accounts for energy dissipation. The force by the spring part is a function of the overlap and for the dashpot is related to the relative velocity of particles at the contact point. In the nonlinear Hertzian contact law, the coefficients for spring stiffness and damping can be functions of particle material properties which change with overlap [Hertz, 1882; Di Renzo and Di Maio, 2004]. In this contact law, the normal and tangential contact forces are calculated as follows [Goniva et al., 2012; Kloss et al., 2012]:

$$F_{pn} = -k_{pn} \delta \varepsilon_{pn} + c_{pn} \delta u_{pn}, \quad (3)$$

$$F_{pt} = \min \left\{ \left| k_{pt} \int_{t_{c,0}}^t \delta u_{pt} dt + c_{pt} \delta u_{pt} \right|, \mu_c F_{pn} \right\}. \quad (4)$$

In equations (3) and (4), k_{pn} and k_{pt} are the normal and tangential spring stiffness, respectively, c_{pn} and c_{pt} are the normal and tangential damping coefficient, respectively, $\delta \varepsilon_{pn}$ is the overlap, and δu_{pn} and δu_{pt} are relative normal and tangential velocities of two particles in contact, respectively. The parameter μ_c in equation (4) is the interparticle friction coefficient that limits the tangential contact force based on the Coulomb friction criteria when particles start sliding over each other. The integral term in equation (4) calculates the force in an incremental spring that stores energy due to relative tangential motion. This incremental spring represents the elastic tangential deformation from the time when two particles touch each other ($t_{c,0}$). The damping part is added to the tangential force component if the Coulomb criterion is not met. For more details about DEM, we refer to the supporting information [Koch and Sangani, 1999; Koch and Hill, 2001; Di Renzo and Di Maio, 2004; Hu et al., 2010; Goniva et al., 2012].

2.2. CFD-DEM

In this paper, we use the unresolved CFD-DEM, where one CFD cell contains several particles as shown in Figure 1a. In this CFD approach, particles are not resolved and only their interaction with the fluid phase is

modelled. In CFD-DEM, the Navier-Stokes equations of fluid mass and momentum conservation are modified considering void fraction due to the presence of the particles as well as the momentum source due to particle motions leading to a two-way coupling between the particle system and the fluid system [Zhou *et al.*, 2010]. Equations (5) and (6) describe the fluid mass and momentum conservation:

$$\frac{\partial(\varepsilon_f)}{\partial t} + \nabla \cdot (\varepsilon_f \cdot u) = 0 \quad (5)$$

$$\frac{\partial(\rho_f \varepsilon_f u)}{\partial t} + \nabla \cdot (\rho_f \varepsilon_f \cdot uu) = -\varepsilon_f \nabla p + F_{pf} + \varepsilon_f \nabla \cdot \tau \quad (6)$$

where ε_f is the fluid volume fraction, ρ_f is the fluid density (assumed constant for the incompressible fluid water), u is the fluid velocity, p is the fluid pressure, and τ is the shear stress tensor of the fluid phase. The term F_{pf} is the momentum exchange between particles and fluid. This momentum exchange term is calculated for each fluid cell and is based on particle drag force.

The momentum exchange between particle and fluid is calculated as follows:

$$F_{pf} = \frac{1}{\Delta V} \sum_{i=1}^n (f_{p,f})_i, \quad (7)$$

where $(f_{p,f})_i$ is the drag force on particle i from the surrounding fluid, where n particles are in the CFD cell and ΔV stands for the CFD cell volume. For the calculation of $(f_{p,f})_i$, different drag force relations have been proposed during recent years [Goniva *et al.*, 2012]. We employ the Koch-Hill drag model that has been shown to give better results for intermediate porosities, in contrast to the commonly applied Gidaspow approach [Koch and Hill, 2001]. For more details of drag correlation as well as CFD-DEM coupling algorithm, see supporting information.

The drag force is also considered as fluid-particle interaction force in the DEM model as well as the force related to pressure gradient and the viscous force [Zhou *et al.*, 2010]. The latter forces are calculated as

$$f_p^p = -V_p \nabla p, \quad (8)$$

$$f_p^v = -V_p \nabla \cdot \tau, \quad (9)$$

where V_p is the particle volume, p is fluid pressure, and τ is the shear stress tensor of the fluid.

3. Numerical Setup

Figure 2 illustrates the DEM model of granular fault gouge composed of 7996 spherical particles with radius ranging between 45 and 75 μm with a uniform distribution. This polydisperse distribution is chosen to be within the range used in the experimental studies performed in the laboratory earthquake machine on glass beads [Scuderi *et al.*, 2014; Scuderi *et al.*, 2015a]. The sample size in our simulations is $11 \times 1.5 \times 0.8$ mm that is equivalent to $6.7d_p$ in depth (direction y in Figure 2), $12.5d_p$ in height (direction z in Figure 2), and $91.7d_p$ in length (direction x in Figure 2), respectively, where d_p is mean particle diameter, 120 μm . We remark that as a guideline, previous numerical simulations have shown that the nature of stick-slip dynamics and distribution of slip event size remains almost unchanged for different sample sizes if appropriate size (equal to or bigger than $4d_p$) is produced in depth of such granular fault gouge [Ferdowsi *et al.*, 2013; Ferdowsi, 2014].

On the sample top and bottom, there are two corrugated plates with high surface roughness modeled by a friction coefficient of 0.9 between plates and particles to facilitate the transmission of shear stresses to the granular gouge. On the front and back sides of the sample, we have frictionless walls with the same elastic properties of particles to avoid a rigid wall boundary conditions. Periodic boundary conditions are applied at the left and right sidewalls representing a long fault gouge in x direction. As mentioned before, the nonlinear Hertzian contact model for the particle interaction force is applied in the normal direction, and the tangential contact force is limited using the Coulomb friction law. The interparticle friction coefficient equals 0.1, which is somewhat smaller than that generally used in the literature for numerical simulations and material used in experiments [Griffa *et al.*, 2013; Ferdowsi *et al.*, 2014; Scuderi *et al.*, 2015a], but allows for larger slip events and reduces the frequency of small fluctuations in macroscopic friction signal [Ferdowsi, 2014]. The employed friction coefficient is the same for dry and saturated models and therefore

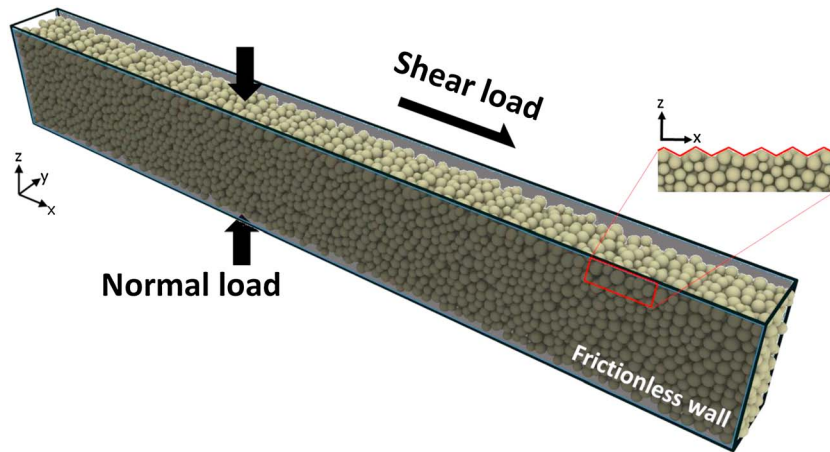


Figure 2. DEM model of the granular fault gouge layer composed of 7996 spherical particles. Image was produce with the open source visualization tool (OVITO) [Stukowski, 2010].

does not play a role in the comparison between dry and saturated models. The full description of material and computational properties is presented in Table 1. Note that when a restitution coefficient of 1.0 is chosen, there is no loss of energy when the particles collide.

Confining stress and shear velocity are the most important parameters controlling shear dynamics of granular materials [Nasuno et al., 1998; Aharonov and Sparks, 2004]. We conducted a phase-space study varying confining stress between 50 kPa and 15 MPa and the shear velocity between 0.006 and 60 mm/s to delineate the different regimes, i.e., steady sliding, slow slip, and stick-slip. Based on this study, we select a confining stress of 10 MPa (z direction) and a shear velocity of 0.6 mm/s to achieve stick-slip behavior. The load is close to that applied in the experimental studies we are interested in simulating [Scuderi et al., 2014; Scuderi et al., 2015a]; however, we use higher shear velocity to gather more slip events in the stick-slip regime (lab studies employ a shear rate of ~5 μm/s).

We use a realistic particle density of 2900 kg/m³ that makes the applied time step for DEM calculations 15e-9 s. This time step is 0.1 to 0.3 times the Rayleigh time, leading to an inertial number 1e-9, assuring that the simulation is a quasi-static flow [MiDi, 2004; Sheng et al., 2004; Agnolin and Roux, 2007]. The gouge is saturated with water, an incompressible Newtonian fluid in the laminar regime. The fluid domain has the same dimensions as the DEM domain, with boundary conditions of no slip for the front-back and top-bottom walls. Boundary conditions at the sidewalls (left and right) are modelled as pressure inlet/outlet boundary conditions allowing inflow or outflow in the granular gouge. The time step for the CFD simulations is 15e-7 s. For stability reasons, the Courant-Friedrichs-Lewy number is continuously monitored to remain within an acceptable range of <1 [Anderson, 1995]. A grid sensitivity analysis is performed to determine the smallest size of CFD cell needed to attain mesh-independent results. In addition, the cell size should be sufficiently large enough such that there are enough particles in each cell (three to five particles per cell) in unresolved CFD-DEM [Goniva et al., 2012; Kloss et al., 2012]. We also performed a sensitivity analysis regarding the time interval when information is exchanged between DEM and CFD, termed the “coupling time interval.” Based on this sensitivity study, the coupling interval is set equal to 1000 DEM time steps. We use the open

Table 1. Material and Numerical Setup Properties

Property	Value	Property	Value
Normal load	10 MPa	Sample size	11 × 1.5 × 0.8 mm
Shear velocity	600 μm/s	Particle radius	45–75 μm
Fluid density	1000 kg/m ³	Particle density	2900 kg/m ³
Fluid viscosity	1e-3 Pa.s	Number of particles	7996
CFD time step	10-7 s	Particle Poisson ratio	0.25
DEM time step	10-9 s	Particle Young's modulus	65 GPa
Coupling interval	10-6 s	Particle friction coefficient	0.1
Number of CFD cell	1760	Particle restitution coefficient	0.87

source software LIGGGHTS [Kloss *et al.*, 2012] for the DEM solver, OpenFOAM [Weller *et al.*, 1998] for the CFD calculations, and CFDEMcoupling [Goniva *et al.*, 2012] to couple the two models. To prepare the sample, particles are inserted randomly in space descending with an initial velocity. Next, the upper plate is displaced downward to apply a normal load to confine the sample. At this stage, the normal load increases until the desired confining stress of 10 MPa is attained. The position of the upper plate is adapted continuously as in the lab experiment in order to maintain the confining stress constant. At constant confining stress, shearing is initiated by moving the bottom plate in x direction until reaching maximum shear stress, at which point stick-slip commences.

4. Stick-Slip in Dry and Saturated Granular Fault Gouge

4.1. Dry Granular Fault Gouge

During stick-slip, we record the macroscopic friction coefficient defined as the ratio of shear stress to the imposed confining stress. We also record the total kinetic energy, which is the sum over all particles of their translational and rotational kinetic energies. The translational kinetic energy of a particle is computed as $\frac{1}{2}m_p v_p^2$ with m_p and v_p being the particle mass and velocity, respectively, and the rotational kinetic energy is computed as $\frac{1}{2}I_p \omega_p^2$ where I_p and ω_p are moment of inertial and angular velocity of particle, respectively, both totalized for all particles. We also record the relative thickness change defined as the difference between the instantaneous and average thickness for the entire simulation normalized by average thickness. The released kinetic energy, drop in friction coefficient, and layer thickness are all used as indicators for the size of a slip event following different former DEM stick-slip studies [Griffa *et al.*, 2013; Ferdowsi *et al.*, 2014].

Figures 3a, 3b, and 3d show a brief but characteristic time series of the macroscopic friction coefficient, kinetic energy of particles, and relative thickness change of the granular fault gouge. Figure 3c shows the ratio between rotational and total particle kinetic energy. In the stick phase, after a brief linear portion, the shear stress increases in a nonlinear manner reaching an almost constant shear stress before approaching slip (Figure 3a). The maximum macroscopic friction coefficient for long periods is found to range between 0.24 and 0.26. At the end of the stick phase, a sudden drop in the friction coefficient occurs. A slip event is characterized by a sudden increase in particle kinetic energy (Figure 3b). The external work is applied to the granular fault gouge by sliding the bottom plate at constant velocity. This work results in an increase of the potential energy stored through the contacts between the particles, meaning that a portion of potential energy is released into particle kinetic energy. From Figure 3c, it is clear that during the slip events, the released particle kinetic energy is primarily translational, amounting to around 80% of the total kinetic energy. This panel also shows that during the stick phase the total kinetic energy consists mainly of rotational kinetic energy (99%) showing that particles are dominantly rotating with respect to each other. Figure 3d shows that the granular gouge layer dilates during the stick phase and compacts during the slip event. The dilatational behavior may be attributed to particle rolling, while the compaction corresponds to a significant rearrangement of the particles due to particle translations. However, note that the relative thickness change is only on the order of 0.2%. Finally, quite small events characterized by small drops in friction coefficient and small increase in particle kinetic energy precede large events, shown in the red box insets of Figures 3a and 3b. We identify these events as microsips. These microsips were also observed in previous numerical studies as well as experiments recorded with acoustic emission techniques showing an exponential increase in frequency approaching major slip events [Ferdowsi *et al.*, 2013; Johnson *et al.*, 2013].

4.2. Comparison of Dry and Saturated Granular Fault Gouge

In this section, we compare the stick-slip behavior for dry and fluid-saturated granular fault gouge. We use identical samples with identical initial particle arrangements for the dry and fluid-saturated models. We shear the sample in the dry state until maximum shear stress is reached. Then we add fluid (time t_0) initiating the coupled CFD-DEM simulation. The saturation process should be looked at as a numerical process, which is immediate and where particles do not change position and no fluid pressure is introduced. In Figures 4a–4c the macroscopic friction coefficient signal, total kinetic energy, and relative thickness change are presented for dry and fluid-saturated models. The total kinetic energy for the fluid-saturated case comprises both particles and fluid kinetic energy, the latter computed as $\frac{1}{2}m_f u_f^2$ where m_f and u_f are the fluid mass and velocity, respectively.

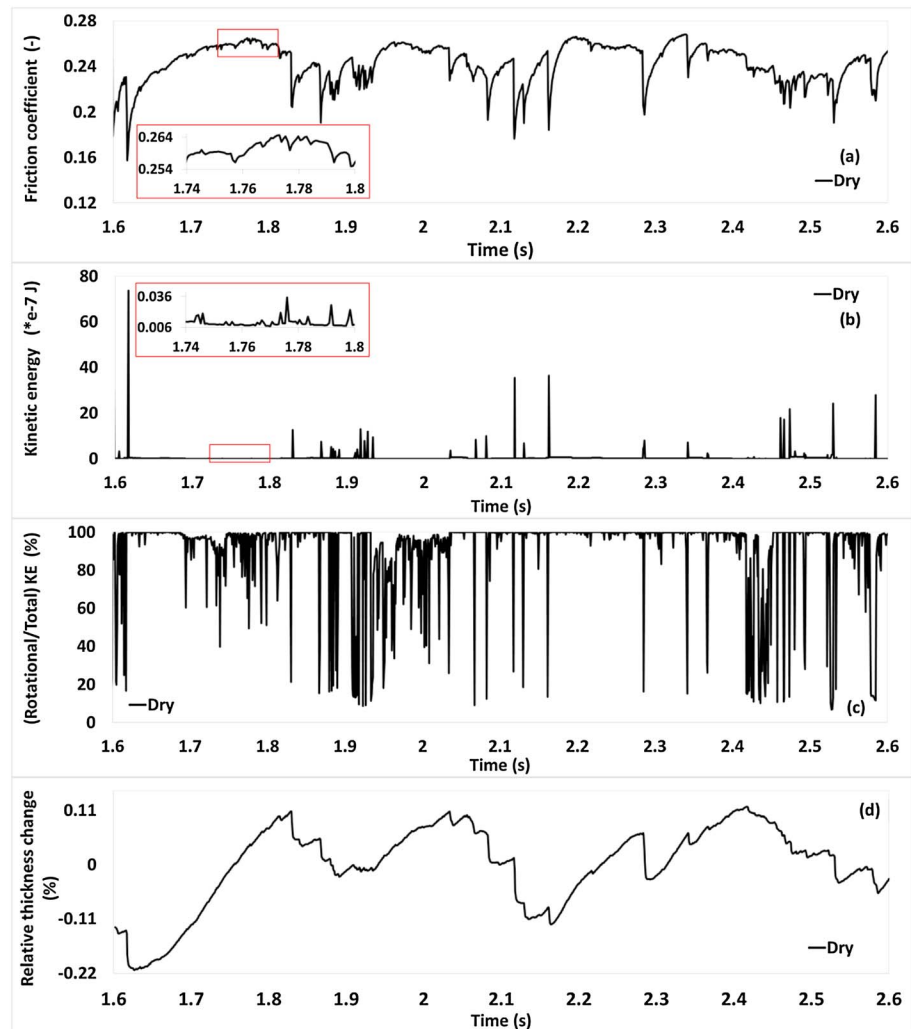


Figure 3. Output of a representative model run with a constant shear driving rate of 0.6 mm/s and normal load of 10 MPa. (a) Macroscopic friction coefficient determined by summing the shear force at the layer boundary and dividing by the layer normal force, (b) total particle kinetic energy summed over the layer for all particles, (c) rotational/total particle kinetic energy ratio, and (d) measured change of layer thickness normalized by the average thickness of layer. The red box insets in Figures 3a and 3b show occurrence of microslips before major slip events.

We observe that the stick-slip behavior is roughly similar for dry and fluid-saturated samples; however, the timing and the size of slip events is changed. In both dry and saturated cases, the friction coefficient increases nonlinearly during the stick phase until reaching a maximum friction coefficient before slip. At slip time, we observe a drop in friction coefficient, an increase in total kinetic energy, and decrease of thickness for both dry and saturated cases. The slip event in the saturated case is accompanied by an increase of the fluid kinetic energy, meaning that the fluid is moving considerably during slip, while it is essentially immobile during stick phase. Next, we present an analysis of long time trains of slip events for dry and fluid-saturated granular fault gouge. We remark that in order to exclude effects of sample preparation, we simulate several samples with different initial particles realizations, i.e., different arrangements of particles in the sample, while the particle size distribution and particle properties are kept unchanged. This procedure insures that our results are statistically independent of sample preparation. The results presented here are found to be representative for all samples. In our analysis, slip events are identified using a drop in friction coefficient with a threshold value ≥ 0.01 . This threshold is chosen sufficiently small to identify small events but large enough to avoid selecting microslips. A second criterion is based on a sufficient high release of particle kinetic energy greater than $0.5e-7$ J. This criterion is used to avoid including small events, which are only due to fluctuations in friction coefficient due to rearrangements of particles during the stick phase. These thresholds are chosen

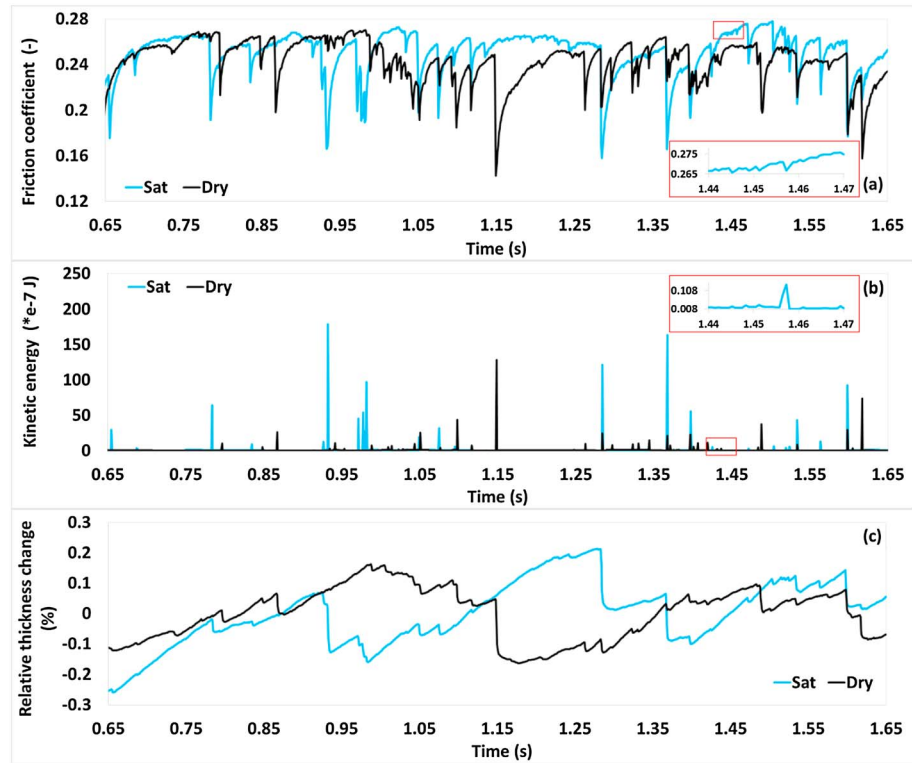


Figure 4. Comparison of (a) macroscopic friction coefficient, (b) total kinetic energy, and (c) relative thickness change of dry and saturated granular fault gouge. Red boxes show occurrence of microslips before major slip events.

after careful analysis of a large number of stick-slip events for different samples. Based on thresholds, around 240 slip events are selected from long simulations of dry and fluid-saturated materials. The complementary cumulative size distribution (cCDF) is defined as

$$cCDF(Y < Y_0) = CDF(Y > Y_0) = 1 - CDF(Y < Y_0) \tag{10}$$

where Y represents the drop in friction coefficient, the release in total kinetic energy, and change in thickness and recurrence time.

Figure 5a shows the cCDF of total kinetic energy release for dry and fluid-saturated case. We observe that the spectrum of event sizes for the saturated case has an increased large kinetic energy release tail. This means that the number of events with large kinetic energy release is larger in the saturated case. The average kinetic energy release increased from dry case ($22e-7$ J) to saturated case ($45e-7$ J). The distribution for saturated case starts to deviate from the dry for events with kinetic energy release higher than $10e-7$ J. Figure 5b shows the cCDF of friction coefficient drop for dry and fluid-saturated case. The saturated case shows in general relatively larger decreases in friction coefficient. The average drop in friction coefficient is lower for the dry case (0.035) compared to that of saturated case (0.045). Figure 5c shows the cCDF of thickness change for dry and fluid-saturated model. We observe that the presence of fluid leads to an increased tail with higher thickness changes during slip events. The average value of decrease of thickness equals $0.419 \mu\text{m}$ for fluid-saturated case in comparison to $0.398 \mu\text{m}$ for dry case. In Figure 6d the cCDF of recurrence time for dry and fluid-saturated granular gouge is shown. We observe an increase in average recurrence time from dry case (0.031 s) to the fluid-saturated case (0.041 s).

5. Discussion

To summarize, we observe that the stick-slip behavior for dry and saturated cases is different, where in the saturated case a higher probability is observed of slip events with higher kinetic energy release, larger drop in friction coefficient, and change in thickness compared to the dry case. To better understand the correlation

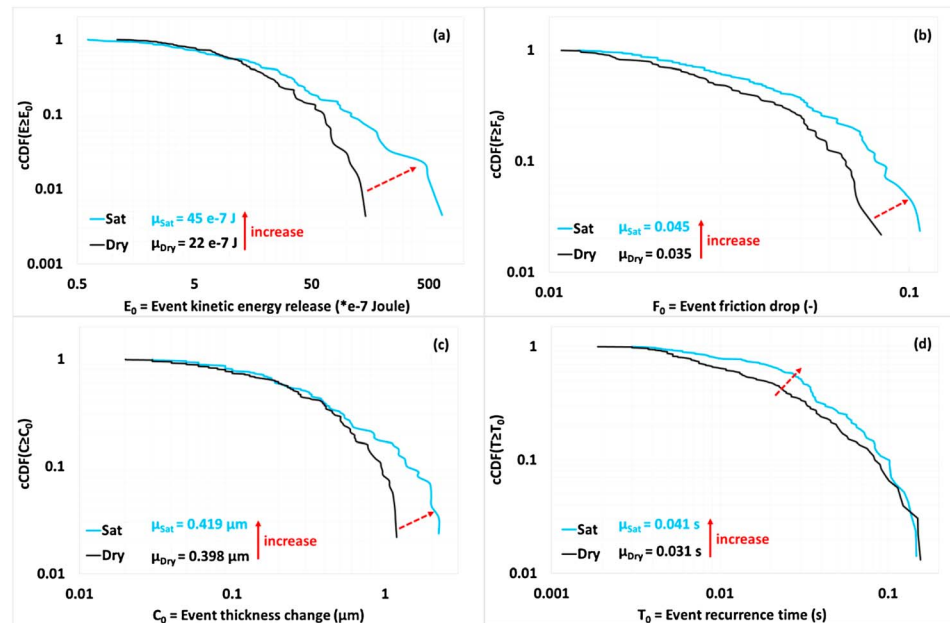


Figure 5. Complementary cumulative size distribution function (cCDF) for dry and saturated granular fault gouge: (a) total kinetic energy release, (b) drop in friction coefficient, (c) thickness change, and (d) recurrence time. Values in figures (μ) indicate average values.

between kinetic energy release, friction coefficient drop, and thickness change, we plot in Figures 6a–6d the relationship between these variables for both dry and fluid-saturated gouge. We observe a power-function-like correlation showing that a large drop in friction coefficient correlates to a high kinetic energy release and change in thickness. Although a significant spread is observed, the values of the correlation coefficients are higher than 0.7 and 0.8 showing, for this highly random process of slips, a clear correlation between the different metrics of slip.

A key observation is that the recurrence time between slip events is longer for the fluid-saturated case compared to the dry case. We determined also the total external work done to the system by integrating

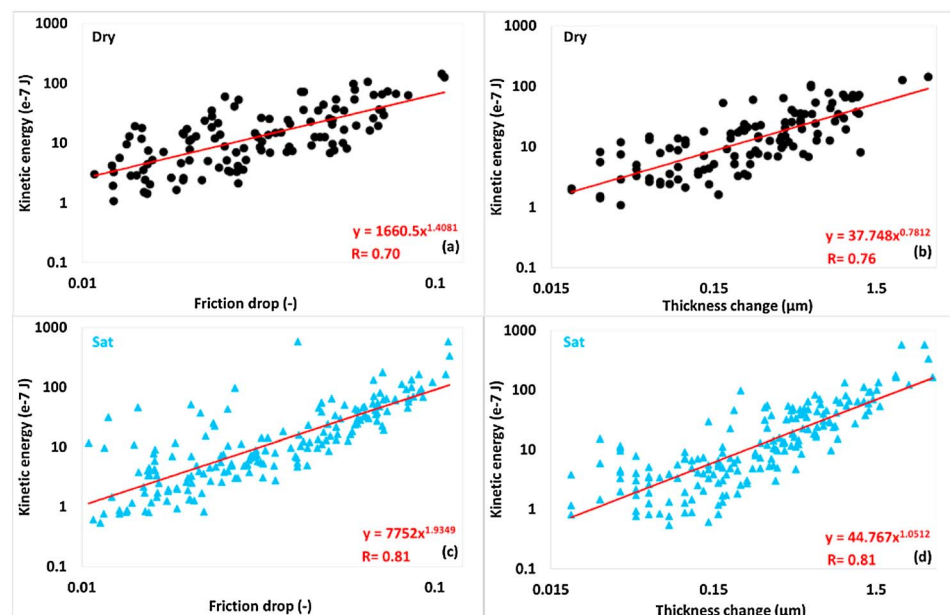


Figure 6. Correlation between characteristics of slip events for (a and b) dry and (c and d) fluid-saturated granular gouge.

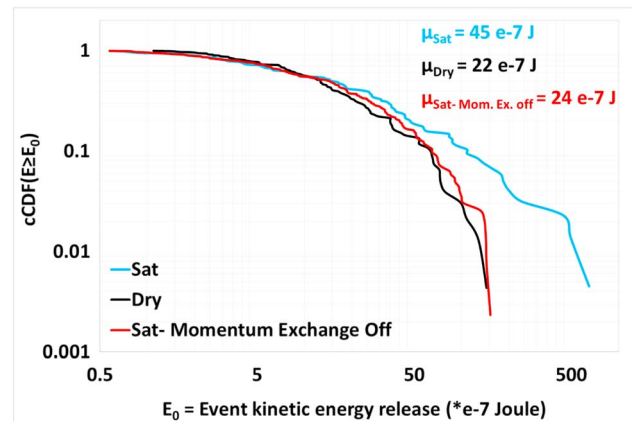


Figure 7. Complementary cumulative size distribution function (cCDF) for dry and saturated granular fault gouge for released total kinetic energy. The red curve is for fluid-saturated fault gouge without momentum exchange between fluid and solid phases.

the product of shear stress with the constant driving shear velocity for both dry and fluid-saturated models. We observed that the external work done is approximately equal for the two systems. That means that for longer recurrence times or equivalently longer stick phases in the saturated case more external work is done on the fault gouge during the stick phase. Accordingly, before a slip event occurs, more energy is stored in the fault gouge in the fluid-saturated case compared to the dry case. Considering this increase in stored energy, and applying the conservation of energy, more energy will be released during slip in the fluid-saturated case.

This leads to the general conclusion that

slip events are larger in the fluid-saturated case, since the fluid stabilizes the granular layer during the stick phase and makes it longer.

We observed that particles during slip are mobilized mainly in translational mode as indicated by the increase in translational particle kinetic energy. In the saturated case, along with an increase in particle kinetic energy, there is also an increase in fluid kinetic energy. This means that the fluid flows with higher velocities during slip, and because we have free inlet/outlet conditions, fluid can flow into or out of the system. This abrupt increase in fluid velocity is found to be related to an abrupt increase in particle velocity during the slip event. The fluid motion during slip can be explained by a momentum exchange from the rapid moving particles to the fluid. In turn, fluid flow may influence particle motion due to drag forces from fluid on particle, forces on particles due to pressure gradient, and viscous forces. We refer to this as a “squirt flow-like” mechanism. To verify the presence of such mechanism, we perform a supplementary statistical analysis of long time train simulation in the fluid-saturated case, where we turn off the drag forces in equations (1) and (6), while other particle-fluid interactions like porosity change, forces from fluid on particles due to pressure gradient, and viscous forces are still considered. Figure 7 shows the cCDF of total kinetic energy release for dry and fluid-saturated case, and fluid-saturated case without considering drag forces. We observe that the saturated case without drag force does not show an increased tail of large kinetic energy release and nearly collapses to the cCDF of the dry sample. This supports our mechanism hypothesis that particle motion during slip induces a fluid motion, which in turn by drag force increases particle motion.

Finally, we note that our numerical simulation results are supported by similar experimental and numerical observations. It has been shown that the presence of a fluid during the stick phase can lead to stabilization of the granular fault gouge and a delay in its slip [Yamashita, 1999; Higashi and Sumita, 2009; Niemeijer et al., 2010]. Also, fluid assisted slip is recognized as an explanation for bigger slip size in fluid-saturated gouge by Bizzarri [2012] and Scuderi et al. [2015a]. These observations confirm our numerical findings of longer recurrence time and larger slip events in the fluid-saturated case. Further, in our simulations we observed almost equal maximum friction coefficients for dry and saturated samples, while the drops in friction coefficient are larger for saturated case compared to the dry case leading to lower minimum friction after slip event for the saturated case. Similar observations are reported in the numerical and experimental studies [Bizzarri, 2012; Scuderi et al., 2015a].

6. Conclusions

Coupled 3-D DEM-CFD simulations are performed to analyze statistically the stick-slip behavior of fluid-saturated granular fault gouge and to compare these with results on dry fault gouge. Fluid flow is modeled using computational fluid dynamics based on the Navier-Stokes equations for an incompressible fluid and

modified to take into account the presence of particles in an unresolved approach. The main findings of this study can be summarized as follows:

Slip events in the fluid-saturated granular fault gouge are characterized by an increase in kinetic energy release and drop in friction coefficient and thickness of the gouge layer compared to the dry case. These three observable variables are found to be highly correlated.

The presence of fluid in the granular fault gouge increases the recurrence time between the slip events. Consequently, more energy is stored between the events leading to higher releases in energy during slip. This leads to larger slip events in the fluid-saturated case compared to the dry case.

The increased kinetic energy release in the fluid-saturated granular fault gouge stems from fluid-particle interaction forces. During a slip event, particles movement leads to a momentum transfer from particles to fluid due to fluid-particle drag forces causing an increase in fluid motion, which in turn enhances the particle motion leading to higher release in kinetic energy. We term this a squirt flow-like mechanism.

In future, we will perform detailed investigations at the grain scale, to better understand the grain-scale mechanisms at play during slip in a fluid-saturated granular fault gouge such as the fluid flow, the corresponding fluid-particle interaction forces, and their effects.

Acknowledgments

Omid Dorostkar would like to thank Dominique Derome for helpful discussions. Support from the technical teams regarding the high performance computational clusters of Empa (Hypatia) and ETH Zurich (Brutus and Euler) is highly appreciated. The authors thank ETH Zurich for funding this study. Paul Johnson and Robert Guyer were also funded by the US DOE Office of Science. Our data are available by FTP transfer by contacting the corresponding author.

References

- Achtziger-Zupančič, P., S. Loew, A. Hiller, and G. Mariethoz (2016), 3D fluid flow in fault zones of crystalline basement rocks (Poehla-Tellerhaeuser Ore Field, Ore Mountains, Germany), *Geofluids*, *16*(4), 688–710, doi:10.1111/gfl.12192.
- Agnolin, I., and J. N. Roux (2007), Internal states of model isotropic granular packings. I. Assembling process, geometry, and contact networks, *Phys. Rev. E*, *76*(6), doi:10.1103/PhysRevE.76.061302.
- Aharonov, E., and D. Sparks (2004), Stick-slip motion in simulated granular layers, *J. Geophys. Res.*, *109*, B09306, doi:10.1029/2003JB002597.
- Anderson, J. D. (1995), *Computational fluid dynamics: The basics with applications*, pp. 153–165, McGraw-Hill, New York.
- Anthony, J. L., and C. Marone (2005), Influence of particle characteristics on granular friction, *J. Geophys. Res.*, *110*, B08409, doi:10.1029/2004JB003399.
- Bizzarri, A. (2012), The mechanics of lubricated faults: Insights from 3-D numerical models, *J. Geophys. Res.*, *117*, B05304, doi:10.1029/2011JB008929.
- Brace, W. F., and J. D. Byerlee (1966), Stick-slip as a mechanism for earthquakes, *Science*, *153*(3739), 990–992, doi:10.1126/science.153.3739.990.
- Cundall, P. A., and O. D. Strack (1979), A discrete numerical model for granular assemblies, *Géotechnique*, *29*(1), 47–65.
- Di Renzo, A., and F. P. Di Maio (2004), Comparison of contact-force models for the simulation of collisions in DEM-based granular flow codes, *Chem. Eng. Sci.*, *59*(3), 525–541, doi:10.1016/j.ces.2003.09.037.
- Dieterich, J. H., and G. Conrad (1984), Effect of humidity on time-dependent and velocity-dependent friction in rocks, *J. Geophys. Res.*, *89*(NB6), 4196–4202, doi:10.1029/JB089iB06p04196.
- Ferdowsi, B. (2014), *Discrete element modeling of triggered slip in faults with granular gouge: Application to dynamic earthquake triggering*, PhD dissertation, ETH Zurich.
- Ferdowsi, B., M. Griffa, R. A. Guyer, P. A. Johnson, C. Marone, and J. Carmeliet (2013), Microslips as precursors of large slip events in the stick-slip dynamics of sheared granular layers: A discrete element model analysis, *Geophys. Res. Lett.*, *40*, 4194–4198, doi:10.1002/grl.50813.
- Ferdowsi, B., M. Griffa, M. Guyer, R. A. Johnson, P. A. Johnson, C. Marone, C., and Carmeliet, J. (2014), Three-dimensional discrete element modeling of triggered slip in sheared granular media, *Phys. Rev. E*, *89*(4), 042204, doi:10.1103/PhysRevE.89.042204.
- Ferdowsi, B., M. Griffa, R. A. Guyer, P. A. Johnson, C. Marone, and J. Carmeliet (2015), Acoustically induced slip in sheared granular layers: Application to dynamic earthquake triggering, *Geophys. Res. Lett.*, *42*, 9750–9757, doi:10.1002/2015GL066096.
- Frye, K. M., and Marone, C. (2002), Effect of humidity on granular friction at room temperature, *J. Geophys. Res.*, *107*(B11), 2309, doi:10.1029/2001JB000654.
- Goniva, C., C. Kloss, N. G. Deen, J. A. M. Kuipers, and S. Pirker (2012), Influence of rolling friction on single spout fluidized bed simulation, *Particuology*, *10*(5), 582–591, doi:10.1016/j.partic.2012.05.002.
- Goren, L., E. Aharonov, D. Sparks, and R. Toussaint (2011), The mechanical coupling of fluid-filled granular material under shear, *Pure Appl. Geophys.*, *168*(12), 2289–2323, doi:10.1007/s00024-011-0320-4.
- Griffa, M., Ferdowsi, B., Guyer, R. A., Daub, E. G., Johnson, P. A., Marone, C., and Carmeliet, J. (2013), Influence of vibration amplitude on dynamic triggering of slip in sheared granular layers, *Phys. Rev. E*, *87*(1), 012205, doi:10.1103/PhysRevE.87.012205.
- Guo, Y. G., and J. K. Morgan (2004), Influence of normal stress and grain shape on granular friction: Results of discrete element simulations, *J. Geophys. Res.*, *109*, B12305, doi:10.1029/2004JB003044.
- Hertz, H. (1882), Ueber die berührung fester elastischer körper, *J. Reine Angew. Math.*, *92*, 156–171.
- Higashi, N., and I. Sumita (2009), Experiments on granular rheology: Effects of particle size and fluid viscosity, *J. Geophys. Res.*, *114*, B04413, doi:10.1029/2008JB005999.
- Hu, G., Z. Hu, B. Jian, L. Liu, and H. Wan (2010), On the determination of the damping coefficient of non-linear spring-dashpot system to model Hertz contact for simulation by discrete element method, in *Proceedings of the 2010 WASE International Conference on Information Engineering*, vol. 3, pp. 295–298.
- Johnson, P. A., and X. Jia (2005), Nonlinear dynamics, granular media and dynamic earthquake triggering, *Nature*, *437*(7060), 871–874, doi:10.1038/nature04015.
- Johnson, T., F. T. Wu, and C. H. Scholz (1973), Source parameters for stick-slip and for earthquakes, *Science*, *179*(4070), 278–280, doi:10.1126/science.179.4070.278.

- Johnson, P. A., H. Savage, M. Knuth, J. Gombert, and C. Marone (2008), Effects of acoustic waves on stick-slip in granular media and implications for earthquakes, *Nature*, *451*(7174), 57–U55, doi:10.1038/nature06440.
- Johnson, P. A., B. Carpenter, M. Knuth, B. M. Kaproth, P. Y. Le Bas, E. G. Daub, and C. Marone (2012), Nonlinear dynamical triggering of slow slip on simulated earthquake faults with implications to Earth, *J. Geophys. Res.*, *117*, B04310, doi:10.1029/2011JB008594.
- Johnson, P. A., B. Ferdowsi, B. M. Kaproth, M. Scuderi, M. Griffa, J. Carmeliet, R. A. Guyer, P.-Y. Le Bas, D. T. Trugman, and C. Marone (2013), Acoustic emission and microslip precursors to stick-slip failure in sheared granular material, *Geophys. Res. Lett.*, *40*, 5627–5631, doi:10.1002/2013GL057848.
- Kaproth, B. M., M. Kaciewicz, S. Muhuri, and C. Marone (2016), Permeability and frictional properties of halite-clay-quartz faults in marine-sediment: The role of compaction and shear, *Mar. Pet. Geol.*, *78*, 222–235, doi:10.1016/j.marpetgeo.2016.09.011.
- Kloss, C., C. Goniva, A. Hager, S. Amberger, and S. Pirker (2012), Models, algorithms and validation for open source DEM and CFD-DEM, *Prog. Comput. Fluid Dyn.*, *12*(2–3), 140–152.
- Koch, D. L., and R. J. Hill (2001), Inertial effects in suspension and porous-media flows, *Annu. Rev. Fluid Mech.*, *33*, 619–647, doi:10.1146/annurev.fluid.33.1.619.
- Koch, D. L., and A. S. Sangani (1999), Particle pressure and marginal stability limits for a homogeneous monodisperse gas-fluidized bed: Kinetic theory and numerical simulations, *J. Fluid Mech.*, *400*, 229–263, doi:10.1017/s0022112099006485.
- Leclère, H., D. Faulkner, J. Wheeler, and E. Mariani (2016), Permeability control on transient slip weakening during gypsum dehydration: Implications for earthquakes in subduction zones, *Earth Planet. Sci. Lett.*, *442*, 1–12, doi:10.1016/j.epsl.2016.02.015.
- Losert, W., J. C. Geminard, S. Nasuno, and J. P. Gollub (2000), Mechanisms for slow strengthening in granular materials, *Phys. Rev. E*, *61*(4), 4060–4068, doi:10.1103/PhysRevE.61.4060.
- Mair, K., and J. F. Hazzard (2007), Nature of stress accommodation in sheared granular material: Insights from 3D numerical modeling, *Earth Planet. Sci. Lett.*, *259*(3–4), 469–485, doi:10.1016/j.epsl.2007.05.006.
- Mair, K., Frye, K. M., and Marone, C. (2002), Influence of grain characteristics on the friction of granular shear zones, *J. Geophys. Res.*, *107*(B10), 2219, doi:10.1029/2001JB000516.
- Marone, C. (1998a), The effect of loading rate on static friction and the rate of fault healing during the earthquake cycle, *Nature*, *391*(6662), 69–72, doi:10.1038/34157.
- Marone, C. (1998b), Laboratory-derived friction laws and their application to seismic faulting, *Annu. Rev. Earth Planet. Sci.*, *26*, 643–696, doi:10.1146/annurev.earth.26.1.643.
- Marone, C., C. B. Raleigh, and C. H. Scholz (1990), Frictional behavior and constitutive modeling of simulated fault gouge, *J. Geophys. Res.*, *95*(B5), 7007–7025, doi:10.1029/JB095iB05p07007.
- MiDi, G. D. R. (2004), On dense granular flows, *Eur. Phys. J. E: Soft Matter Biol. Phys.*, *14*(4), 341–365, doi:10.1140/epje/i2003-10153-0.
- Morgan, J. K. (1999), Numerical simulations of granular shear zones using the distinct element method—2. Effects of particle size distribution and interparticle friction on mechanical behavior, *J. Geophys. Res.*, *104*(B2), 2721–2732, doi:10.1029/1998JB900055.
- Nasuno, S., A. Kudrolli, A. Bak, and J. P. Gollub (1998), Time-resolved studies of stick-slip friction in sheared granular layers, *Phys. Rev. E*, *58*(2), 2161–2171, doi:10.1103/PhysRevE.58.2161.
- Niemeijer, A., C. Marone, and D. Elsworth (2010), Frictional strength and strain weakening in simulated fault gouge: Competition between geometrical weakening and chemical strengthening, *J. Geophys. Res.*, *115*, B10207, doi:10.1029/2009JB000838.
- Okazaki, K., I. Katayama, and H. Noda (2013), Shear-induced permeability anisotropy of simulated serpentinite gouge produced by triaxial deformation experiments, *Geophys. Res. Lett.*, *40*, 1290–1294, doi:10.1002/grl.50302.
- Proctor, B., and G. Hirth (2015), Role of pore fluid pressure on transient strength changes and fabric development during serpentine dehydration at mantle conditions: Implications for subduction-zone seismicity, *Earth Planet. Sci. Lett.*, *421*, 1–12, doi:10.1016/j.epsl.2015.03.040.
- Renard, F., S. Beaupretre, C. Voisin, D. Zigone, T. Candela, D. K. Dysthe, and J. P. Gratier (2012), Strength evolution of a reactive frictional interface is controlled by the dynamics of contacts and chemical effects, *Earth Planet. Sci. Lett.*, *341*, 20–34, doi:10.1016/j.epsl.2012.04.048.
- Samuelson, J., C. Marone, B. Voight, and D. Elsworth (2008), Laboratory investigation of the frictional behavior of granular volcanic material, *J. Volcanol. Geotherm. Res.*, *173*(3–4), 265–279, doi:10.1016/j.jvolgeores.2008.01.015.
- Samuelson, J., D. Elsworth, and C. Marone (2009), Shear-induced dilatancy of fluid-saturated faults: Experiment and theory, *J. Geophys. Res.*, *114*, B12404, doi:10.1029/2008JB006273.
- Scuderi, M. M., and Collettini, C. (2016), The role of fluid pressure in induced vs. triggered seismicity: Insights from rock deformation experiments on carbonates, *Sci. Rep.*, *6*, 24852, doi:10.1038/srep24852.
- Scuderi, M. M., B. M. Carpenter, and C. Marone (2014), Physicochemical processes of frictional healing: Effects of water on stick-slip stress drop and friction of granular fault gouge, *J. Geophys. Res. Solid Earth*, *119*, 4090–4105, doi:10.1002/2013JB010641.
- Scuderi, M. M., B. M. Carpenter, P. A. Johnson, and C. Marone (2015a), Poromechanics of stick-slip frictional sliding and strength recovery on tectonic faults, *J. Geophys. Res. Solid Earth*, *120*, 6895–6912, doi:10.1002/2015JB011983.
- Scuderi, M. M., H. Kitajima, B. M. Carpenter, D. M. Saffer, and C. Marone (2015b), Evolution of permeability across the transition from brittle failure to cataclastic flow in porous siltstone, *Geochem. Geophys. Geosyst.*, *16*, 2980–2993, doi:10.1002/2015GC005932.
- Sheng, Y., C. J. Lawrence, B. J. Briscoe, and C. Thornton (2004), Numerical studies of uniaxial powder compaction process by 3D DEM, *Eng. Comput.*, *21*(2–4), 304–317, doi:10.1108/02644400410519802.
- Stukowski, A. (2010), Visualization and analysis of atomistic simulation data with OVITO—The open visualization tool, *Modell. Simul. Mater. Sci. Eng.*, *18*(1), doi:10.1088/0965-0393/18/1/015012.
- Sutherland, R., et al. (2012), Drilling reveals fluid control on architecture and rupture of the alpine fault, New Zealand, *Geology*, *40*(12), 1143–1146, doi:10.1130/g33614.1.
- Verberne, B. A., C. J. Spiers, A. R. Niemeijer, J. H. P. De Bresser, D. A. M. De Winter, and O. Plummer (2014), Frictional properties and microstructure of calcite-rich fault gouges sheared at sub-seismic sliding velocities, *Pure Appl. Geophys.*, *171*(10), 2617–2640, doi:10.1007/s00024-013-0760-0.
- Weller, H. G., G. Tabor, H. Jasad, and C. Fureby (1998), A tensorial approach to computational continuum mechanics using object-oriented techniques, *Comput. Phys.*, *12*(6), 620–631, doi:10.1063/1.168744.
- Yamashita, T. (1999), Pore creation due to fault slip in a fluid-permeated fault zone and its effect on seismicity: Generation mechanism of earthquake swarm, *Pure Appl. Geophys.*, *155*(2–4), 625–647, doi:10.1007/s000240050280.
- Zhou, Z. Y., S. B. Kuang, K. W. Chu, and A. B. Yu (2010), Discrete particle simulation of particle–fluid flow: Model formulations and their applicability, *J. Fluid Mech.*, *661*, 482–510, doi:10.1017/s002211201000306x.